Journal of Molecular Liquids 265 (2018) 327–336

Contents lists available at ScienceDirect

Journal of Molecular Liquids

journal homepage: www.elsevier.com/locate/molliq

Thermal, microstructural, and spectroscopic analysis of Ca^{2+} alginate/clay nanocomposite hydrogel beads☆,☆☆

Renan da Silva Fernandes [a], Márcia Regina de Moura [a], Greg M. Glenn [b], Fauze Ahmad Aouada [a,*]

[a] Grupo de Compósitos e Nanocompósitos Híbridos (GCNH), Department of Physics and Chemistry, Programa de Pós-Graduação em Ciência dos Materiais, São Paulo State University (Unesp), School of Engineering, Ilha Solteira, 15385-000 Ilha Solteira, SP, Brazil
[b] Bioproduct Research Unit, USDA-ARS, WRRC, Albany, CA 94710, United States

ARTICLE INFO

Article history:
Received 28 March 2018
Received in revised form 23 May 2018
Accepted 2 June 2018
Available online 4 June 2018

Keywords:
Hydrogels
Nanocomposites
Nanoclay
Zeolite
Sodium alginate

ABSTRACT

Polymeric hydrogels are important biomaterials with potential for various applications including the controlled release of drugs. Clay and zeolite nanostructures can enhance the absorption and release properties of hydrogels. In our previous work, a procedure was optimized for making hydrogel beads. The objectives of this study were to use the optimized bead forming procedure to prepare clay and zeolite nanocomposite hydrogel beads and characterize their microstructure, thermal and chemical properties. The hydrogels were prepared by dripping solutions of either sodium alginate or sodium alginate/nanostructure (clay and/or zeolite) into beakers containing different concentrations of $CaCl_2$ at 25 °C. Fourier transform infrared spectroscopy (FTIR) analysis detected the presence of functional groups associated with alginate, clay and zeolite. The microstructure of the alginate beads was somewhat rough with small protrusions. Flakes were visible in micrographs of beads containing nanoclay. The elemental composition of the hydrogels was investigated by energy dispersive X-ray spectrometry (EDX). EDX spectra revealed magnesium, sodium, aluminum, silicon and increased the levels of oxygen in the nanoclay compositions. The incorporation of nanoclays decreased the percentage of organic matter lost as detected by thermogravimetric analysis (TG). TG was also able to detect the incorporation of nanoclay in hydrogels. The nanoclays proved to be more effective than zeolites in producing alginate hydrogels with satisfactory swelling characteristics.

1. Introduction

Various polymers used in biomedical applications have important functional properties including biocompatibility and biodegradability [1]. Some polymers can be classified as biomaterials precisely for such properties. Moreover, in human trials their performance is very satisfactory. Polymers can even be used in prosthetic devices where they prove to be highly functional and can displace high-cost equipment [2].

Among the materials designated as polymers, alginate is a polysaccharide of particular interest. In addition to the benefits already highlighted above, alginate is hydrophilic in nature, has low toxicity, and is relatively inexpensive [3, 4]. The alginate polymer is composed of linear chains of α-L-guluronic acid (G) and β-D-manuronic acid (M) blocks identified as rigid and flexible blocks, respectively. Alginate is extracted from brown algae (*Phaeophyceae*) [5].

Alginate is particularly useful in the production of firm hydrogels through the use of multi-valent cations [6]. When exposed to multi-valent cations, the alginate chains begin to interact with the ions that form crosslinks with other nearby chains. This characteristic crosslinking behavior with multi-valent cations is a key to the formation of alginate hydrogels. Several studies also describe the preparation of hydrogels formed by crosslinking alginate with other polymers [7–9]. For instance, Facchi et al. [7] prepared hydrogel beads by using a steady drip of alginate solution into a slowly stirred chitosan solution.

Hydrogels are polymeric materials known particularly for the ability to absorb high amounts of water in their three-dimensional structure. In contrast to hydrogels that are chemically crosslinked to form covalent bonds and do not dissolve after the chemical reaction is complete, hydrogels that are crosslinked with ionic bonds can dissolve depending on the external factors to which it is exposed, such as changes in pH, temperature, saline solutions, among others [10]. The softness and flexibility of hydrogels contribute to their wide use in biomedicine, they are mainly used to deliver medications that reduce inflammation and discomfort in patients. Other uses of hydrogels within the medical field include their use in contact lenses and for tissue engineering (bone regeneration), healing ointments, drug coating, and controlled delivery systems [11–13]. There are many studies that report the effective use of hydrogels containing nanostructures. Nanostructures such as nanoparticles have been shown to improve the absorption and release of active

☆ The authors declare that there is no conflict of interest regarding the publication of this article.
☆☆ This article belongs to VSI:14th CBPol/Special Issue.
* Corresponding author.
E-mail address: faouada@yahoo.com.br (F.A. Aouada).

https://doi.org/10.1016/j.molliq.2018.06.005
0167-7322/

agents. Among the nanoparticles studied, clays and zeolites are the most common. Clays and zeolites are materials classified as minerals that are naturally formed by geological events and hydrothermal variations of volcanic lavas, respectively. Clays and zeolites are generally considered to be non-toxic when ingested [14]. Several applications for alginate-clay and alginate-zeolite nanocomposites have been reported [15–17].

Clay minerals have a sheet-like structure and are mainly composed of tetrahedrally arranged silicate and octahedrally arranged aluminate groups. The sheet-like structures form platelets that remain bound together by means of the van der Waals forces and relatively weak polar forces. Among these platelets are cationic metals that are compacted due to internal electrostatic forces [14, 18]. Today, hydrogels are valued in applications that exploit their absorption capacity, chemical inertness, low toxicity, and their ability to control the release of various pharmaceuticals [19, 20]. Zeolites are minerals that are porous, comprised mostly aluminosilicate and are used as adsorbents and catalysts as well as in medical applications [21]. Various studies have shown zeolites to be highly effective for topical wound dressings, kidney dialysis, and diarrheal drugs, and have shown antitumor, antimicrobial, and antiviral activity and are of interest in controlled drug release systems [22].

In our previous work, a procedure was optimized for making hydrogel beads. The effect of nanoparticle concentration on bead formation and the hydrophilic and structural properties of the beads were investigated [23]. In other related works, there are several reports about alginate-Ca hydrogels and some about alginate-Ca-clay hydrogels that mainly relate to their application [24–27]. For instance, the work described by Iliescu et al. [27] studied the preparation and characterization of clay and sodium alginate nanocomposite beads used for the controlled release of irinotecan. The main objective was the incorporation of the irinotecan, and the potential application of this nanocomposite in chemotherapy. A detailed investigation into how the crosslinker, clay and zeolite affect the nanocomposite properties is needed. The objective of this work was to prepare different formulations of sodium alginate hydrogels containing clay and zeolite nanoparticles, and to characterize in detail the possible interactions by Fourier Transform Infrared Spectroscopy (FTIR) and thermogravimetric (TG) techniques.

2. Experimental

2.1. Material and methods

Sodium alginate (SA) was obtained from Cromoline® Química Fina Brazil. Pure anhydrous calcium chloride ($CaCl_2$) was acquired from Sigma-Aldrich. The nanostructures used were the zeolite, Clinoptilolite ZK406 H (St. Cloud Zeolite) and the nanoclay, Cloisite-Na^+ (Southern Clay Products®). The reagents were used as received without any purification.

2.2. Preparation of solutions

2.2.1. Preparation of sodium alginate solutions

A solution of the polysaccharide sodium alginate was made at a concentration of 2% (w/v). The alginate solution was stirred continuously for about 4 h. Afterwards, the solution was stored in the refrigerator to inhibit microbial growth.

2.2.2. Preparation nanoclay and zeolite dispersions

The Cloisite-Na^+ nanoclay dispersions were added at concentrations of 1, 2.5 and 5% (w/v). Initially, the nanoclay was dispersed for 30 min under continuous magnetic stirring. The nanoclay solution was then sonicated in an ultrasonic agitator (Branson Digital Sonifier® Model 450–400 W) by 5 cycles of 1 min each with 50% frequency.

Solutions of zeolite nanoparticles (2.5% and 5%, w/v) were prepared by dispersing in water with continuous stirring after which the solutions were sonicated in 5 cycles of 1 min each with 50% frequency. Subsequently, the zeolite solutions were added to the beaker containing the clay slurry and stirred rigorously until dispersed.

2.3. Preparation of hydrogels

2.3.1. Preparation of calcium alginate nanocomposite hydrogel beads

A syringe pump (New Era model NE-300) was used to extrude a 2% solution (w/v) of sodium alginate or alginate with nanoclay and zeolite nanostructures at a rate of 30 mL/h into beakers containing different concentrations of calcium chloride (1, 2.5 and 5% w/v). The drops of sodium alginate immediately formed beads as they fell into the solutions of calcium chloride. The beads were kept for 2 h in the calcium chloride solution to ensure the crosslinking process had completed. The beads were then collected on a screen, washed and dialyzed for 24 h to remove the excess calcium. Finally, the beads were separated on an acrylic plate and dried at 25 °C.

2.4. Characterization

2.4.1. Fourier Transform Infrared Spectroscopy (FTIR)

FTIR was used to investigate the functional groups of the materials and possible interactions between them. The hydrogel beads were triturated, mixed with potassium bromide (KBr) and pressed to obtain pellets. The spectral range investigated was 4000–400 cm^{-1} accumulating 128 scans with a resolution of 2 cm^{-1} in a spectrophotometer Nicolet - Nexus 670 FTIR.

2.4.2. Scanning Electron Microscopy (SEM) and Energy Dispersive Spectroscopy X-ray (EDX)

SEM (ZEISS, model LS15 EVO) was used to investigate the morphological properties of the hydrogel and nanocomposite beads. The samples were viewed using a voltage of 10, 15 and 20 kV. A secondary electron detector (SE1) was used with a detection and microanalysis module coupled with X-ray energy dispersive (EDX) spectroscopy (resolution of 133 eV). After the purification process, some samples were separated as whole beads and others were cut in half to evaluate the internal morphology. The surfaces of alginate hydrogel beads and their nanocomposites were sputter gold coated before analyses.

2.4.3. Thermogravimetric analyzer (TG)

The equipment used for thermal analysis was TA Instruments TGA Q-500. Approximately 7–10 mg of sample was placed in the TG equipment. The samples were heated from room temperature up to 800 °C at 10 °C/min. The nitrogen gas flow in the TGA was 40.0 mL/min in the balance and 60.0 mL/min in the sample chamber.

3. Results and discussion

3.1. Fourier Transform Infrared Spectroscopy (FTIR)

The effect of different concentrations of Ca^{2+} crosslinker on alginate hydrogels is shown in Fig. 1.

Analyzing the FTIR spectra for sodium alginate revealed a wide band between 3200 and 3600 cm^{-1} corresponding to the stretching of the –OH groups present in the alginate polymer chain. The intense bands observed in 1414 cm^{-1} and 1621 cm^{-1} correlated respectively to the asymmetric and symmetric axial deformations of the $–COO^-$ groups indicating the presence of the carboxylic acid group in the alginate. Silverstein et al. [28] reported that the carboxylate ion generates 2 spectroscopic bands in these regions because the C═O bonds have an intermediate coupling force from C═O and C—O. The 1032 cm^{-1} peak was related to the vibrating motion of the C—C bond as reported in previous studies [29, 30].

FTIR spectra of hydrogel beads crosslinked with Ca^{2+} revealed spectroscopic bands at 1621 and 1414 cm^{-1} that were related to the stretching of $–COO^-$ the majority of which were bonded to Ca^{2+} to

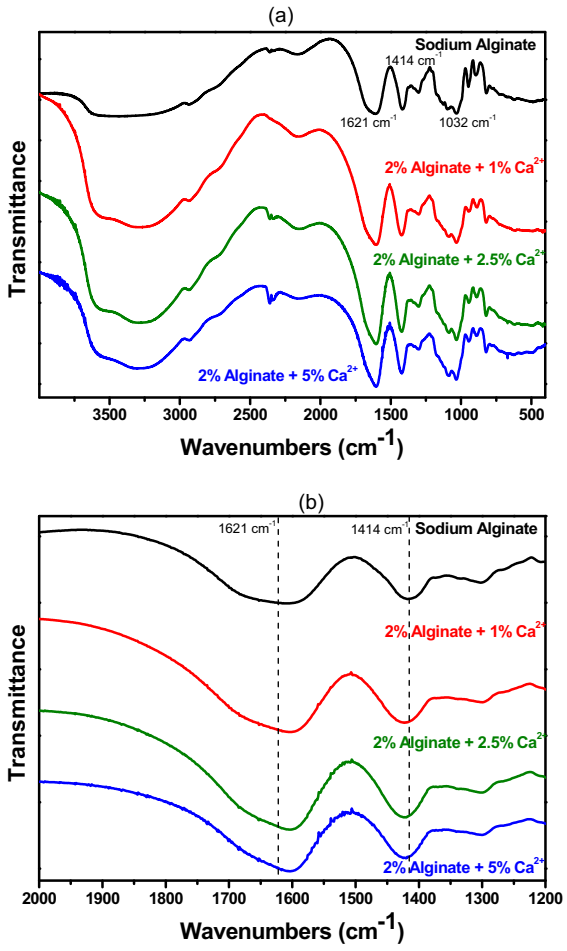

Fig. 1. FTIR spectra of pure sodium alginate and alginate bead hydrogels prepared with different concentrations of calcium in the 400–4000 cm^{-1} region (a) and 1200–2000 cm^{-1} region (b).

form three-dimensional crosslinked networks of hydrogels. Hua et al. [31] reported that the interactions between Ca^{2+} ions with $-COO^{-}$ anionic groups shifted the 1621 and 1414 cm^{-1} peaks to higher wavenumbers. A similar shift was observed in this work where the band at 1414 cm^{-1} (sodium alginate - control) was displaced to 1420 cm^{-1} (hydrogels containing 5% Ca^{2+}). The band at 1621 cm^{-1} was displaced to a lower wavenumber region (1603 cm^{-1}) compared to the sodium alginate spectrum (Fig. 1b, control) further indicating a possible interaction between $-COO^{-}$ and Ca^{2+}. The interaction between these species is further confirmed by the degree of swelling as previously reported [23].

The spectroscopic properties of calcium alginate nanocomposites containing different concentrations of nanoclay and crosslinked with 5% of calcium are shown in Fig. 2.

The FTIR spectra for the nanoclay sample revealed a wide band at 3250–3600 cm^{-1} that was attributed to the elongation (axial deformation) of the structural –OH groups and –OH interleaved. There was also a narrow, strong band at 1641 cm^{-1} related to the angular deformation of the –OH interlayer. The peaks at 1040 cm^{-1} and 976 cm^{-1} were related to Si—O—Si axial deformation into and out of the plane of the tetrahedral site. A low intensity peak at 510 cm^{-1} was attributed to the elongation of the bonds between the Si—O—Al groups. A band centered at 470 cm^{-1} was attributed to the stretching of the Mg—O bond as in previous reports [32, 33].

In relation to the alginate nanocomposites, the Si—O—Si and Si—O—Al bands intensified with increasing nanoclay content. An

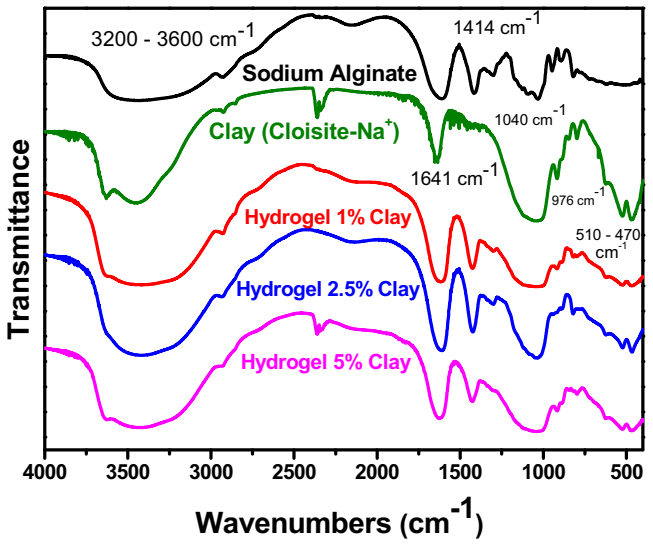

Fig. 2. FTIR spectra of sodium alginate, clay and alginate-clay nanocomposites.

intense broad peak was also observed at 1040 cm^{-1}, which was related to the overlap of C—C bonds of alginate and axial deformation into and out of the Si—O—Si bond plane. In addition, a small peak attributed to axial deformation of the Si—O bond was observed at 976 cm^{-1}. Likely interactions between alginate $-COO^{-}$ groups and the –OH groups present in the clay were confirmed by the slight upward shift of the band around 1600–1700 cm^{-1}. These interaction points are shown in Scheme 1.

FTIR characterization of the nanocomposites prepared with zeolite is shown below (Fig. 3). Regarding the pure zeolite curve, well-defined bands were observed around 3500 cm^{-1} and 1656 cm^{-1}, which is indicative of stretching of the structural –OH groups (Al—OH—Al), (Si—OH—Si) and flexion movement of the O—H—O. The presence of a wide peak in the region of 1070 cm^{-1} and another low intensity peak centered at 600 cm^{-1} refer to the asymmetric stretching vibration of Si—O and Al—O, respectively, in a tetrahedral site. A peak with low intensity associated with the vibration of O—Si—O and O—Al—O was observed at 794 cm^{-1}. Finally, a band was observed at 470 cm^{-1} that was attributed to the vibration of Si—O and Al—O. Similar results were presented by Rashidzadeh et al. [34] and Mansouri et al. [35]. Two main characteristic features were observed in the FTIR spectra that were possibly related to the interaction between the alginate $-COO^{-}$ group and –OH structural zeolite. These features were the bands between 400 and 800 cm^{-1} in the zeolite containing samples that intensified with increasing zeolite content and bands that were displaced to much higher wavenumbers for the alginate carboxyl groups (1612 and 1414 cm^{-1}).

Nanocomposites containing both nanoclays and zeolites were also characterized by FTIR (Fig. 4). The characteristic bands for the nanoclays and zeolites were visible in the FTIR spectra of the composite blends. For instance, the peak centered at 1414 cm^{-1} that related to the asymmetric stretching of the $-COO^{-}$ groups for the sodium alginate component was observed. The nanoclay component was detected by characteristic peaks between 400 and 550 cm^{-1} related to Si—O—Si and Si—O—Al and by the peak at 470 cm^{-1} which was assigned to Mg—O stretching. The zeolite component was detected by the low intensity peak at 794 cm^{-1}. Finally, the fact that nanoclay and zeolite nanostructures are composed of similar atoms, some bands overlapped in certain regions. For instance, the 3300 to 3600 cm^{-1} spectroscopic region related to (–OH) from the water of hydration. The wide bands observed between 1000 and 1100 cm^{-1} related to asymmetrical stretching vibration of Si—O and Al—O in their tetrahedral site and axial deformation into and out of the Si—O—Si plane.

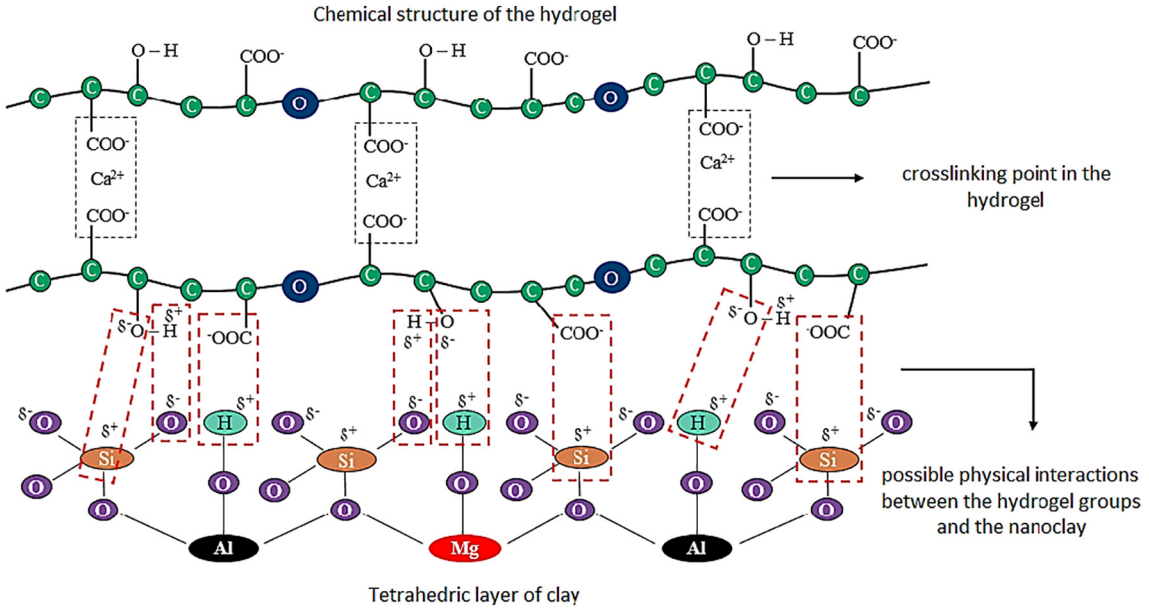

Scheme 1. Proposed scheme indicating the possible interaction points between clay and crosslinked alginate chains.

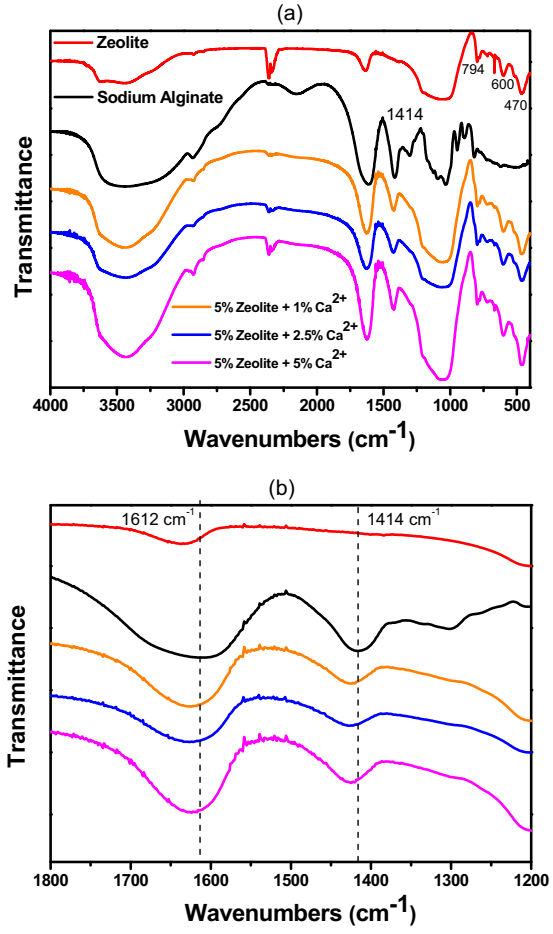

Fig. 3. FTIR spectra of sodium alginate, pure zeolite and nanocomposites prepared with different concentrations of calcium in the 400–4000 cm^{-1} region (a) and 1200–1800 cm^{-1} region (b).

3.2. Scanning Electron Microscopy (SEM)

SEM was used to evaluate the surface properties of pure nanoclay, dehydrated hydrogels and their nanocomposites. Flakes and/or rough bulky layers were observed in some regions from the nanoclay bead surface (Fig. 5). Similar results were reported by Mallakpour and Dinari [36].

SEM micrographs of beads comprised of 2% alginate + 5% $CaCl_2$ show that the roughly spherical beads had a rough surface with various cracks and wrinkles interspersed across the surface. These characteristics are probably artifacts related to the dehydration process of the beads. Similar observations were found by Swamy et al. [37], Bera et al. [38] and Pasparakis et al. [39]. The rough surface of the beads and the presence of cavities (pores) in various sizes and shapes were observed in higher magnification (Fig. 6b). Such cavities could be responsible for water vapor transmission or fluid leakage into and out of the beads. The increase of both the surface roughness (Fig. 6c–d) and internal compaction of the samples (Fig. 6f) was a characteristic feature of calcium alginate hydrogels containing nanoclays. In addition, sub-surface roughness was observed on the inner surface of a bead containing nanoclay that had been cut in half to expose its internal morphology. The roughness may increase the contact surface area of the nanocomposite hydrogels improving, for instance, absorption of water and solutes as reported in previous studies [23, 40, 41]. SEM micrographs of samples containing 2.5 and 5% w/v nanoclay showed features similar to those in Fig. 6c–f and, therefore, were not included.

Macroscopically, the diameter of the hydrogel beads increased with higher concentrations of nanoclay as is illustrated in Fig. 7. The increase was attributed to the higher expansion due to the hydration and swelling of the nanoclay component.

3.3. Energy dispersive X-ray spectrometry (EDX)

The EDX is a semi-quantitative analytical technique that can be used to determine the elemental composition in the different samples. As expected, the pure hydrogels had only carbon, oxygen and calcium elements. The detection of calcium was supportive of the hypothesis that a crosslinked network of calcium alginate had formed. No sodium was detected in the nanocomposites. It may be that the sodium ions diffused out of the beads once the nanoclay hydrated and swelled and the

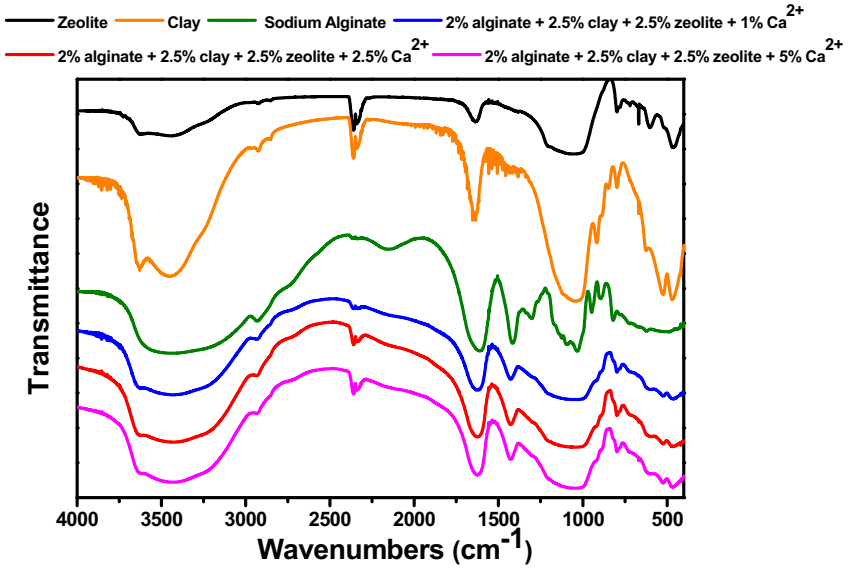

Fig. 4. FTIR spectra of sodium alginate, clay, zeolite and nanocomposites prepared with Ca^{2+} crosslinker concentrations.

alginate polymer chains penetrated the platelets of nanoclay where the sodium ions initially were bound (Scheme 2). EDX was useful in detecting the formation of a calcium alginate nanocomposite that remained stable, even after the dialysis treatment was performed to remove unbound calcium ions.

The EDX data (Table 1) included the elemental composition of the nanoclay used in making the nanoclay alginate hydrogels. Although the EDX technique is only semi-quantitative, it clearly showed higher levels of magnesium, aluminum, silicon and oxygen in the hydrogels containing higher levels of the nanoclay.

3.4. Thermogravimetric (TG) and differential thermogravimetric (DTG) analyses

TG analyses of sodium alginate, pure nanoclay and different nanocomposite formulations were performed to determine the thermal stability of the hydrogels over a given heating profile. The TG and DTG curves of the different hydrogel samples revealed three main thermal events (Fig. 8).

The first event was observed in the range of 30 to 150 °C and was associated with the loss of moisture and other volatiles (Fig. 8). The second event occurred in the temperature range of 200–320 °C and was associated with the decomposition of the alginate carbon chains and the formation of sodium carbonate (Na_2CO_3) as an intermediate product. The last thermal event occurred in the range 600–700 °C and was associated with the decomposition of the Na_2CO_3 in two stages as shown below [42]:

1st decomposition stage : $Na_2CO_{3\ (l)} \rightarrow Na_2O_{(s)} + CO_{2(g)}$

2nd decomposition stage : $Na_2O_{(s)} \rightarrow 2\ Na_{(g)} + 1/2\ O_{2(g)}$

For hydrogels with 1% $CaCl_2$, the same three thermal events were detected but they occurred at a higher temperature range. The 1st event occurred in the temperature range 38–174 °C, the second event occurred in the range of 200 to 390 °C and the third event occurred in the range of 600–735 °C Similar thermal behaviors occurred in alginate samples containing 2.5 and 5% $CaCl_2$. The TG residue after the heating cycle was approximately 30-wt%. This residue was inorganic material that remained stable at high temperatures (800 °C). Similar results were reported by Kumar et al. [43], Eldin et al. [44] and de Paula et al. [45].

Two peaks were observed around 200–350 °C in TG data for hydrogels prepared with 2.5 and 5% Ca^{2+}. In the pure alginate sample and the sample prepared from the lowest calcium concentration, only one peak occurred. The peak was related to the decomposition of free alginate chains or chains with a low degree of entanglement. At higher concentrations of Ca^{2+}, there is an increased amount of crosslinking and chain immobilization. Consequently, the thermal event related to the degradation of these chains shifted to higher temperatures. The increased crosslinking and chain entanglement may increase the hydrophobic interactions in the sample as shown in Scheme 3.

The initial, maximum and final temperatures of the thermal events obtained from the DTG curves (Table 1S) indicate that changes in concentration of Ca^{2+} did not significantly change the

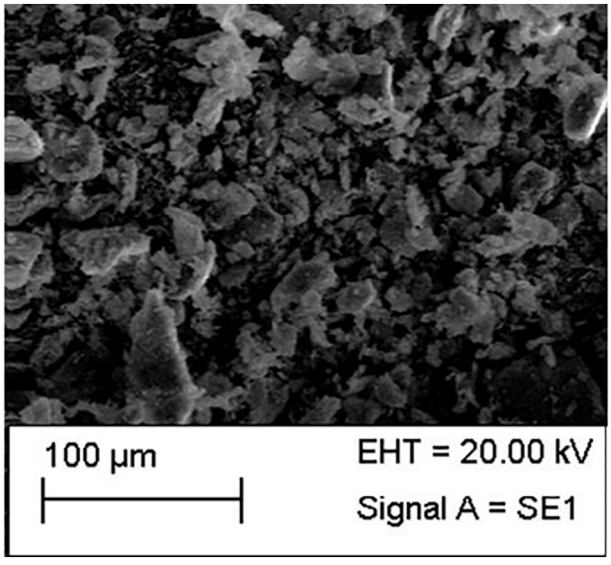

Fig. 5. Electronic micrographics obtained by SEM of the nanoclay cloisite-Na^+ at 300×.

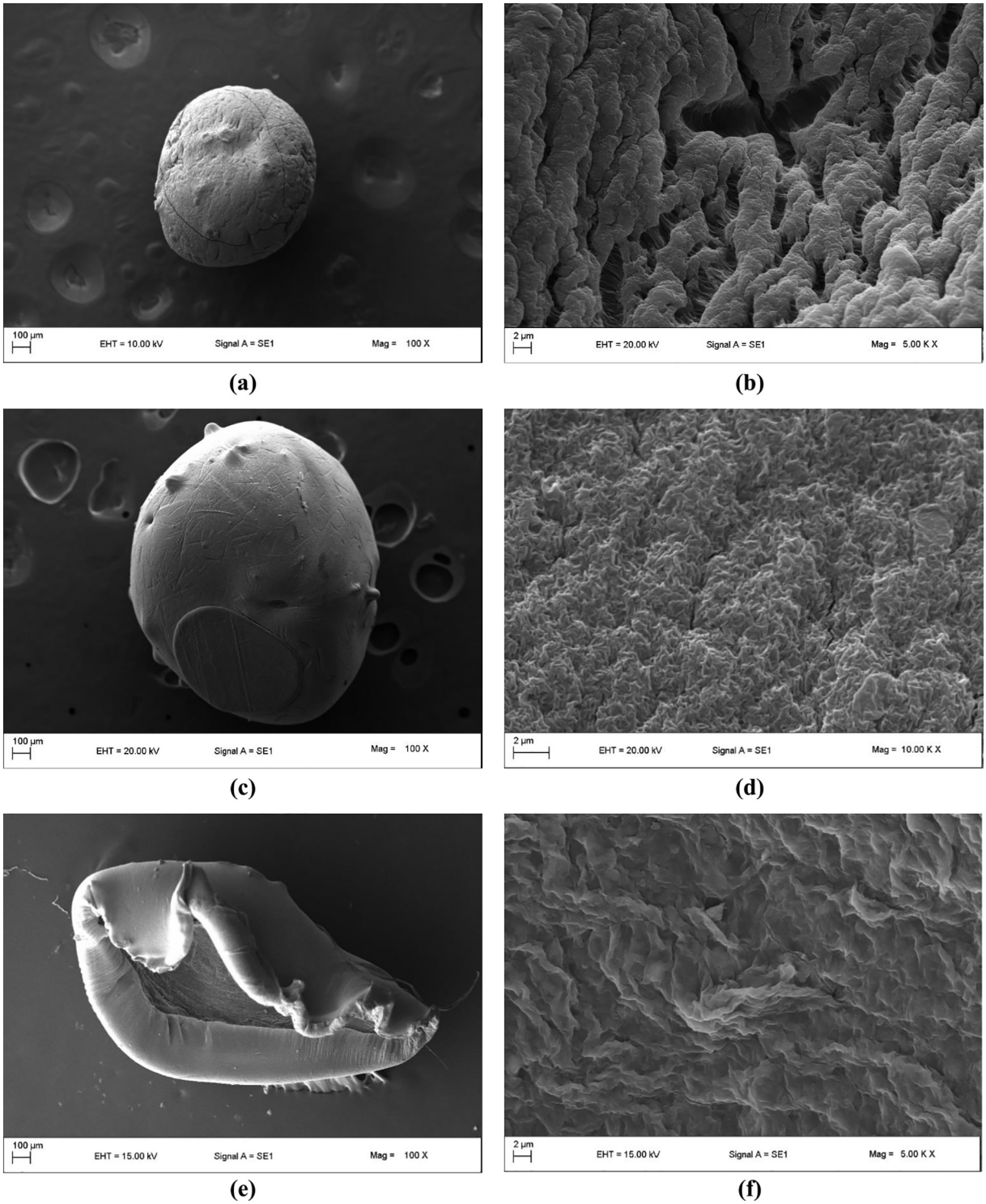

Fig. 6. Surface electronic micrographics obtained by SEM of the alginate hydrogels (a–b), nanocomposites prepared with 1% clay (c–d) and (e–f) internal electronic micrographics of the nanocomposites prepared with 1% clay.

lower end of the temperature range for the second thermal event. However, the rate of degradation decreased with increasing amounts of Ca^{2+}, which demonstrated that the thermal stability of the hydrogels was improved by increasing the concentration of Ca^{2+}.

As seen in Fig. 9a and b, the pure nanoclay had two thermal events. The first thermal event occurred in the temperature range of 34–105 °C. The weight loss from the first thermal event was about 6.5% and was attributed primarily to the volatilization of water (free water). The second thermal event occurred between 560 and 676 °C and resulted in a 2.9% (w/v) weight loss. This weight loss corresponded to dihydroxylation (i.e., breaking of the bonds of the hydroxyl groups ($-OH^-$) that are tightly bonded in the structure of nanoclay [46, 47]). This result was expected since the nanoclay is an inorganic material, and is thermally

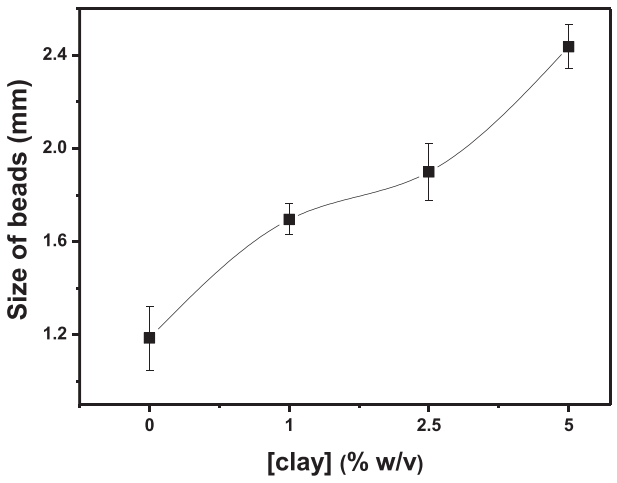

Fig. 7. Effect of clay concentration on size of alginate hydrogel nanocomposites.

stable in this temperature range. Other thermal events that caused significant mass loss required a higher temperature range. The temperature at which the alginate began to thermally degrade with the breaking of the carbonic chains occurred at 212 °C and gradually increased as temperatures increased to 221 °C (Fig. 9c).

Increasing the clay content from 0 to 5%, improved the thermal stability of the nanocomposites. The miscibility of the alginate and nanoclay components would tend to facilitate the movement of hydrated alginate chains into the space between the clay sheets. In this manner, the $-COO^{-}$ groups of the alginate may be interacting with the –OH groups of nanoclay, forming hydrogen bonds that require higher energy to fragment and thus make the nanocomposites more thermally stable. This interaction was previously discussed in the FTIR analysis (Scheme 1). The intercalation of alginate chains into the nanoclay layers effectively protects the organic material (alginate) from the externally applied heat. These factors contribute to the decrease in the thermal degradation rate of the nanoclay composites (Table 1S). Similar results were presented by Rafiei and Ghomi [34] and Iliescu et al. [27].

The mass loss during thermal degradation depended on the concentration of nanoclay in the nanocomposites (Table 2S). However, the effect was more than would be expected based solely on the nanoclay content. For instance, the mass loss of pure alginate hydrogel after thermal degradation, i.e., without nanoclay, was approximately 70%. In contrast, the mass loss of the nanocomposite containing 5% nanoclay was only 30% (Table 2S).

4. Conclusion

Nanocomposite hydrogels can be readily made with nanoclays and zeolites. The nanomaterials used in the hydrogels confer different physicochemical properties. Physical differences such as in surface roughness in hydrogel beads were apparent in SEM micrographs. Chemical differences in the nanocomposite hydrogels were apparent in FTIR analyses of the samples. Thermal stability of the hydrogels was improved by crosslinking with calcium or by the incorporation of nanoclays. The results of this study show that the properties of hydrogels can be modified with nanoclays and zeolites. By strategically modifying the properties of

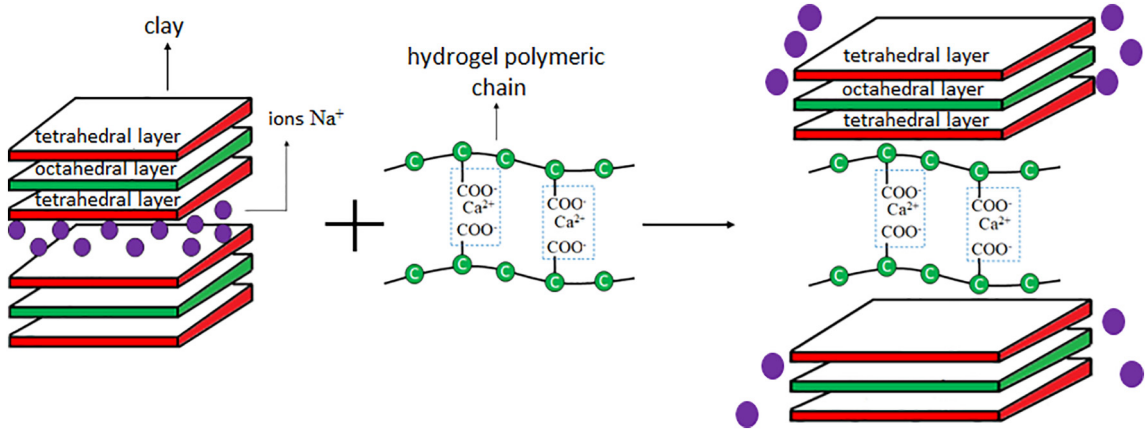

Scheme 2. Hypothetical model of the possible conformation between hydrogel and nanoclay after the nanocomposite formation.

Table 1
Analysis of EDX of the pure hydrogel, clay and nanocomposite prepared with three different clay concentrations.

Materials		Elements						
		Calcium	Carbon	Magnesium	Sodium	Aluminum	Silicon	Oxygen
Nanoclay	% Atomic	–	–	1.0 ± 0.05	2.1 ± 0.01	6.4 ± 0.1	18.4 ± 0.01	71.9 ± 0.1
	% mass	–	–	1.3 ± 0.07	2.6 ± 0.1	9.0 ± 0.1	27.0 ± 0.04	59.9 ± 0.1
Pure hydrogel	% Atomic	7.5 ± 0.2	49 ± 1	–	–	–	–	47 ± 1
	% mass	10.1 ± 0.5	39 ± 1	–	–	–	–	50.5 ± 0.9
Hydrogel/1%nanoclay	% Atomic	2.8 ± 0.7	36 ± 0.8	0.28 ± 0.01	–	1.9 ± 0.3	6 ± 1	54 ± 1
	% mass	7 ± 1	26 ± 1	0.4 ± 0.02	–	3.1 ± 0.3	10 ± 1	53 ± 2
Hydrogel/2.5%nanoclay	% Atomic	2.0 ± 0.1	29 ± 0.5	0.4 ± 0.02	–	5.9 ± 0.1	8.7 ± 0.5	56.5 ± 0.3
	% mass	4.9 ± 0.3	21.0 ± 0.5	0.6 ± 0.02	–	4.8 ± 0.2	14.6 ± 0.7	54.0 ± 0.7
Hydrogel/5%nanoclay	% Atomic	1.3 ± 0.3	25 ± 0.1	0.59 ± 0	–	3.7 ± 0.2	10 ± 1	58 ± 2
	% mass	3.1 ± 0.7	17 ± 2	0.8 ± 0.01	–	5.8 ± 0.4	17.6 ± 0.1	55 ± 3

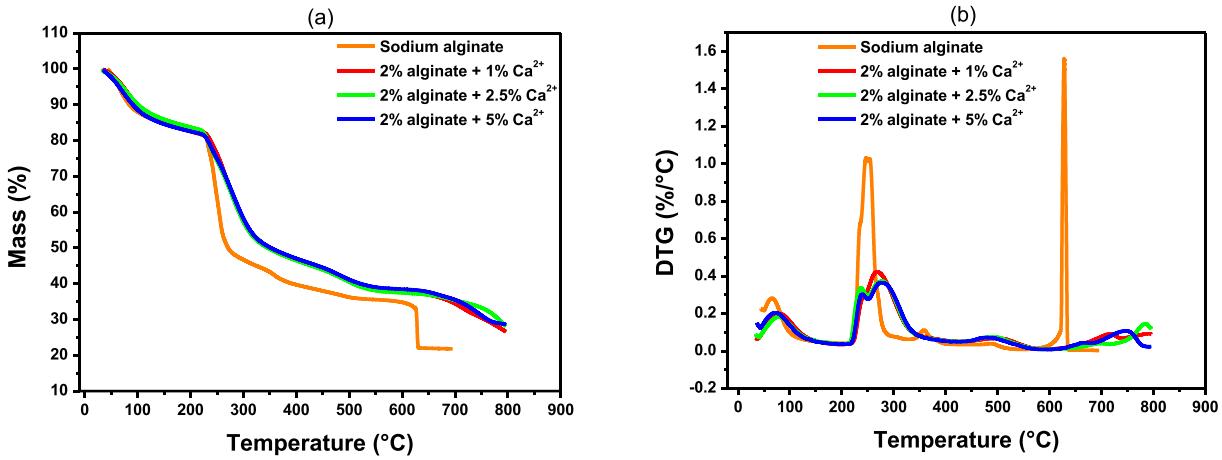

Fig. 8. TG (a) and DTG (b) curves of sodium alginate and alginate hydrogels crosslinked with different Ca^{2+} content.

the hydrogels, their application in the medical field such as in controlled-release medications could be further expanded.

Acknowledgments

The authors are grateful to Universidade Estadual Paulista, and Brazilian research financing institutions Fundação de Amparo à Pesquisa do Estado de São Paulo (FAPESP) (2013/03643-0), Conselho Nacional de Desenvolvimento Científico e Tecnológico (CNPq) (405680/2016-3) and Coordenação de Aperfeiçoamento de Pessoal de Nível Superior (CAPES) for their financial support.

Appendix A. Supplementary data

Supplementary data to this article can be found online at https://doi.org/10.1016/j.molliq.2018.06.005.

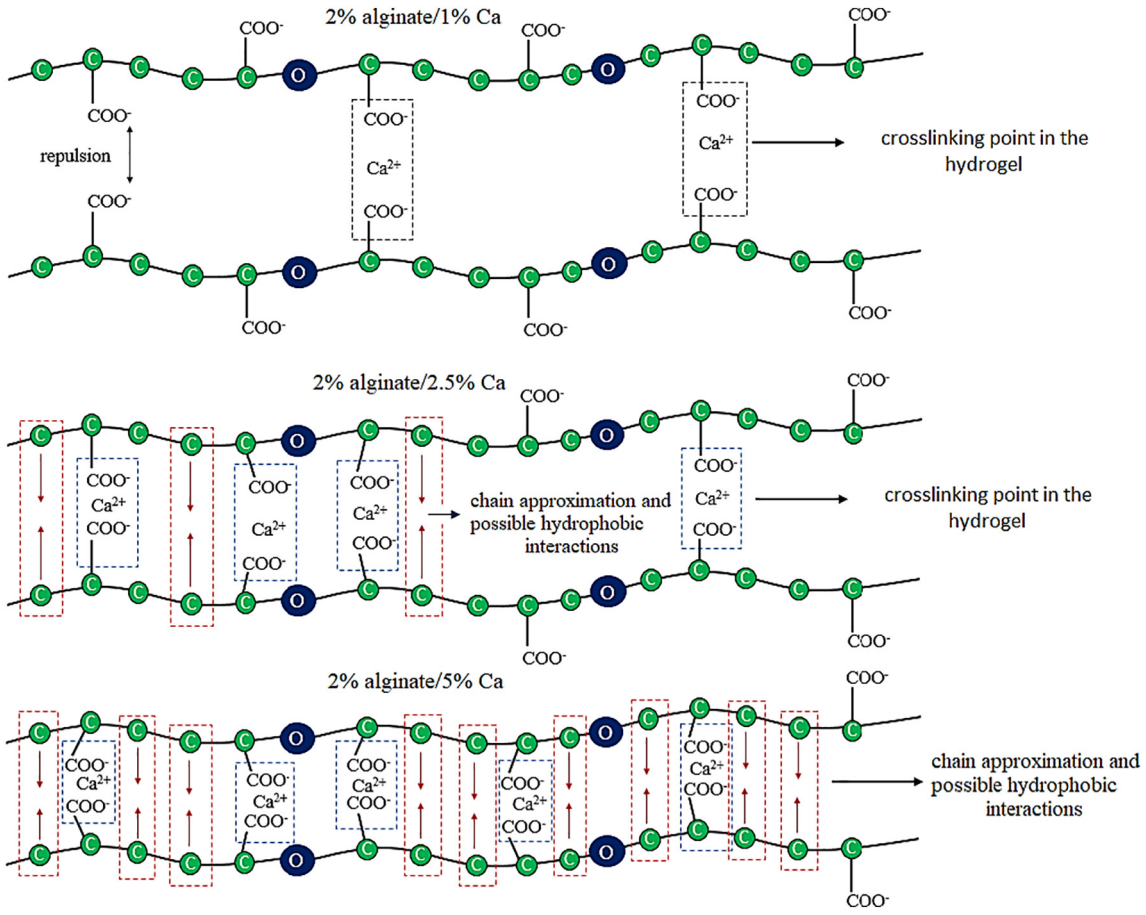

Scheme 3. Hydrostatic crosslinking model and possible hydrophobic interactions between the chains. The green spheres and blue spheres represent the carbon and oxygen atoms of the polymer chain, respectively.

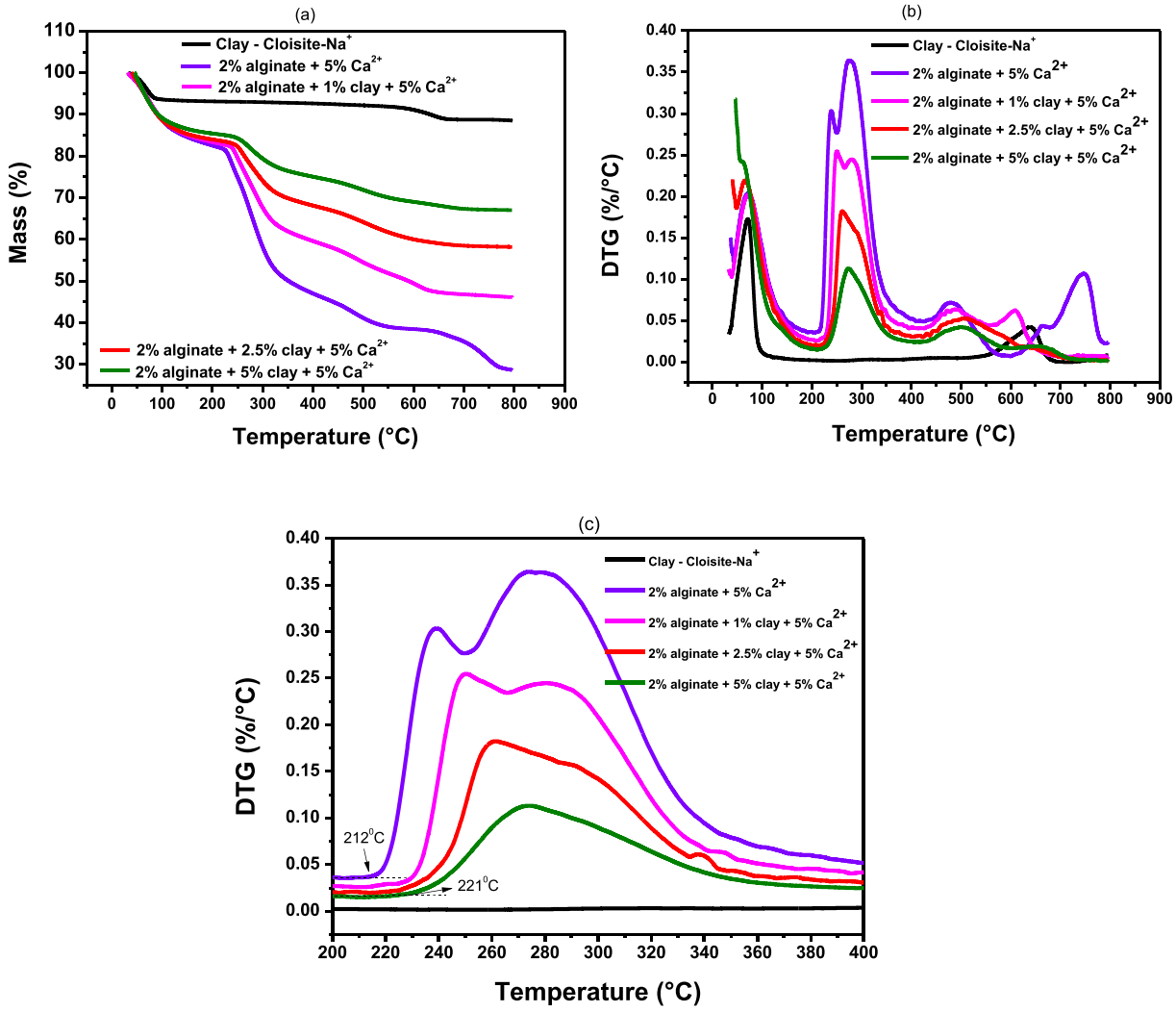

Fig. 9. TG (a), DTG (b) and DTG showing the second thermal event (C) of clay, alginate hydrogels and nanocomposites prepared with different clay content crosslinked with 5% Ca^{2+}.

References

[1] G.C.J. Swarnavalli, V. Kannappan, D. Roopsingh, V. Joseph, Effect of solvent on the size and properties of polymeric nanoparticles of poly(ε-caprolactam), J. Mol. Liq. 236 (2017) 61–67.

[2] F.D. Williams, On the nature of biomaterials, Biomaterials 30 (2009) 5897–5909.

[3] B. Iqbal, N. Muhammad, A. Jamal, P. Ahmad, Z.U.H. Khan, A. Rabin, S.A. Khan, G. Gonfa, J. Iqbal, I.U. Rehman, An application of ionic liquid for preparation of homogeneous collagen and alginate hydrogels for skin dressing, J. Mol. Liq. 243 (2017) 720–725.

[4] K.M. Rao, A. Kumar, A. Haider, S.S. Han, Polysaccharides based antibacterial polyelectrolyte hydrogels with silver nanoparticles, Mater. Lett. 184 (2016) 189–192.

[5] S.N. Pawar, K.J. Edgar, Alginate derivatization: a review of chemistry, properties and applications, Biomaterials 33 (2012) 3279–3305.

[6] J. Composada, P. Gou, B. Marcos, J. Arnau, Physical properties of sodium alginate solutions and edible wet calcium alginate coatings, LWT Food Sci. Technol. 64 (2015) 212–219.

[7] D.P. Facchi, A.L. Cazetta, E.A. Canesin, V.C. Almeida, E.G. Bonafé, M.J. Kipper, A.F. Martins, New magnetic chitosan/alginate/Fe_3O_4@SiO_2 hydrogel composites applied for removal of Pb(II) ions from aqueous systems, Chem. Eng. J. 337 (2018) 595–608.

[8] G. Wang, Z. Wang, L. Huang, Feasibility of chitosan-alginate (Chi-Alg) hydrogel used as scaffold for neural tissue engineering: a pilot study *in vitro*, Biotechnol. Biotechnol. Equip. 31 (2017) 766–773.

[9] E.A. Kamoun, E.-R.S. Kenawy, T.M. Tamer, M.A. El-Meligy, M.S.M. Eldin, Poly (vinyl alcohol)-alginate physically crosslinked hydrogel membranes for wound dressing applications: characterization and bio-evaluation, Arab. J. Chem. 8 (2015) 38–47.

[10] J.O. Gonçalves, J.P. Santos, E.C. Rios, M.M. Crispim, G.L. Dotto, L.A.A. Pinto, Development of chitosan based hybrid hydrogels for dyes removal from aqueous binary system, J. Mol. Liq. 225 (2017) 265–270.

[11] K.Y. Lee, D.J. Mooney, Alginate: properties and biomedical applications, Prog. Polym. Sci. 37 (2012) 106–126.

[12] E.M. Ahmed, Hydrogel: preparation, characterization, and applications: a review, J. Adv. Res. 6 (2015) 105–121.

[13] J.S. Henrique, R.S. Falcare, P.S. Lopes, Artigo: Sistema de liberação controlada, Pharm. Bras. 22 (2006).

[14] É.T. Neto, Â.A.T. Neto, Modificação química de argilas: Desafios científicos e tecnológicos para obtenção de novos produtos com maior valor agregado, Quim Nova 32 (2009) 809–817.

[15] B.H.N. Reddy, P.R. Raut, V. Venkatalakshimi, S. Sreenivasa, Synthesis and characterization of Cloisite-30B clay dispersed poly (acryl amide/sodium alginate)/AgNp hydrogel composites for the study of BSA protein drug delivery and antibacterial activity, Mater. Res. Express. 5 (2018) 3–25.

[16] S. Vahidhabanu, D. Karuppasamy, A.I. Adeogun, B.R. Babu, Impregnation of zinc oxide modified clay over alginate beads: a novel material for the effective removal of Congo red from wastewater, RSC Adv. 7 (2017) 5669–5678.

[17] Y. Wang, M. Luo, F. Xu, W. Zhang, Conversion of Volcanic Tephra to Zeolites for Calcium Ion Cross-linked Alginate-zeolite Composites for Enhanced Aqueous Removal of Cu(II) Ions, 226, 2015 1–13.

[18] L.H. Vieira, V. Rodrigues, L. Martins, Cristalização convencional de zeólitas e induzida por sementes, Quim. Nova. XY, 2014 1–10.

[19] M.I. Carretero, Clay minerals and their beneficial effects upon human health. A review, Appl. Clay Sci. 21 (2002) 155–163.

[20] L.A.S. de Rodrigues, A. Figueiras, F. Veiga, R.M. de Freitas, L.C.C. Nunes, E.C.S. da Filho, C.M.S. da Leite, The systems containing clays and clay minerals from modified drug release: a review, Colloids Surf. B: Biointerfaces 103 (2013) 642–651.

[21] R.T. Rigo, S.B.C. Pergher, D.I. Petkowicz, J.H.Z. dos Santos, Um novo procedimento de síntese da zeólita A empregando argilas naturais, Quim Nova 32 (2009) 21–25.

[22] B. de Gennaro, L. Catalanotti, P. Cappelleti, A. Langella, M. Mercurio, C. Serri, M. Biondi, L. Mayol, Surface modified natural zeolite as a carrier for sustained diclofenac release: a preliminary feasibility study, Colloids Surf. B: Biointerfaces 130 (2015) 101–109.

[23] R.S. Fernandes, M.R. de Moura, F.A. Aouada, Optimization of synthesis of intercalated nanocomposite hydrogels for future application in the medical area, Quim Nova 40 (2017) 60–67.

[24] A. Olad, M. Pourkhiyabi, H. Gharekhani, F. Doustdar, Semi-IPN superabsorbent nanocomposite based on sodium alginate and montmorillonite: reaction parameters and swelling characteristics, Carbohydr. Polym. 190 (2018) 295–306.
[25] R. Fabryanty, C. Valencia, F.E. Soetaredjo, J.N. Putro, S.P. Santoso, A. Kurniawan, Y.-H. Ju, S. Ismadji, Removal of crystal violet dye by adsorption using bentonite-alginate composite, J. Environ. Chem. Eng. 5 (2017) 5677–5687.
[26] A.A. Edathil, P. Pal, F. Banat, Alginate clay hybrid composite adsorbents for the reclamation of industrial lean methyldiethanolamine solutions, Appl. Clay Sci. 156 (2018) 213–223.
[27] R.I. Iliescu, E. Andronescu, C.D. Ghitulica, G. Voicu, A. Ficai, M. Hoteteu, Montmorillonite-alginate nanocomposite as a drug delivery system – incorporation and in vitro release of irinotecan, Int. J. Pharm. 463 (2014) 184–192.
[28] F.X. Webster, in: R.M. Silverstein (Ed.), Spectrometric Identification of Organic Compounds Infrared Spectrometry, sixth ed., 2005 , [Hoboken, New Jersey].
[29] S. Barreca, S. Orecchio, A. Pace, The effect of montmorillonite clay in alginate gel beads for polychlorinated biphenyl adsorption: isothermal and kinetic studies, Appl. Clay Sci. 99 (2014) 220–228.
[30] A. Cvitanovic-B, D. Komes, S. Karlovic, S. Djakovic, I. Spoljaric, G. Mrsic, D. Jezek, Improving the controlled delivery formulations of caffeine in 86 alginate hydrogel beads combined with pectin, carrageenan, chitosan and psyllium, Food Chem. 167 (2015) 378–386.
[31] S. Hua, H. Ma, X. Li, H. Yang, A. Wang, pH – sensitive sodium alginate/poly(vinyl alcohol) hydrogel beads prepared by combined Ca^{2+} crosslinking and freeze-thawing cycles for controlled release of diclofenac sodium, Int. J. Biol. Macromol. 46 (2010) 517–523.
[32] S. Mallakpour, M. Dinari, Biomodification of cloisite-Na^{+} with L-methionine amino acid and preparation of poly (vinyl alcohol)/organoclay nanocomposite films, J. Appl. Polym. Sci. 124 (2011) 4322–4330.
[33] B. Rafiei, F.A. Ghomi, Preparation and characterization of the Cloisite-Na^{+} modified with cationic surfactants, Iran J. Crystall. Mineral. 21 (2013) 25–32.
[34] A. Rashidzadeh, A. Olad, D. Salari, A. Reyhanitabar, On the preparation and swelling properties of hydrogel nanocomposite based on sodium alginate-g-poly (acrylic acid-co-acrylamide)/Clinoptilolite and its application as slow release fertilizer, J. Polym. Res. 344 (2014) (2014).
[35] N. Mansouri, N. Rikhtegar, H.A. Panahi, F. Atabi, B.K. Shahraki, Porosity, characterization and structural properties of natural zeolite – Clinoptilolite – as a sorbent, Environ. Prot. Eng. 39 (2013) 140–152.
[36] S. Mallakpour, M. Dinari, Preparation and characterization of new organoclays using natural amino acids and Cloisite-Na^{+}, Appl. Clay Sci. 51 (2011) 353–359.
[37] B.Y. Swamy, Y.S. Yun, In vitro release of metformin from iron (III) cross-linked alginate-carboxymethyl cellulose hydrogel beads, Int. J. Biol. Macromol. 77 (2015) 114–119.
[38] H. Bera, S.G. Kandukuri, A.K. Nayak, S. Boddupalli, Alginate-sterculia gum gel-coated oil-entrapped alginate beads for gastroretentive risperidone delivery, Carbohydr. Polym. 120 (2015) 74–84.
[39] G. Pasparakis, N. Bouropoulos, Swelling studies and in vitro release of verapamil from calcium alginate and calcium alginate-chitosan beads, Int. J. Pharm. 323 (2006) 34–42.
[40] H. Kaygusuz, F.B. Erim, Alginate/BSA/montmorillonite composites with enhanced protein entrapment and controlled release efficiency, React. Funct. Polym. 73 (2013) 1420–1425.
[41] Q. Wang, J. Zhang, A. Wang, Preparation and characterization of a novel pH-sensitive chitosan-g-poly(acrylic acid)/attapulgite/sodium alginate composite hydrogel bead for controlled release of diclofenac sodium, Carbohydr. Polym. 78 (2009) 731–737.
[42] J.W. Kim, Y.D. Lee, H.G. Lee, Decomposition of Na_2CO_3 by interaction with SiO_2 in mold flux of steel continuous casting, ISIJ Int. 41 (2001) 116–123.
[43] M. Kumar, R. Tamilarasan, G. Arthanareeswaran, A.F. Ismail, Optimization of methylene blue using Ca^{2+} and Zn^{2+} bio-polymer hydrogels beads: a comparative study, Ecotoxicol. Environ. Saf. 121 (2015) 164–173.
[44] M.S.M. Eldin, E.A. Kamoun, M.A. Sofan, S.M. Elbayomi, L-Arginine grafted alginate hydrogel beads: a novel pH-sensitive system for specific protein delivery, Arab. J. Chem. 8 (2015) 355–365.
[45] H.C.B. de Paula, E.F. de Oliveira, F.O.M.S. Abreu, R.C.M. de Paula, S.M. de Morais, M.M.C. Forte, Esferas (beads) de alginato como agente encapsulante de óleo de cróton zehntneri pax et hoffm, Polímeros, 20, 2010 112–120.
[46] F.Q. Mariani, J.C. Villalba, F.J. Anaissi, Caracterização estrutural de argilas utilizando DRX com luz Síncrotron, MEV, FTIR e TG-DTG-DTA, Orbital Elec. J. Chem. 5 (2013) 249–256.
[47] I.F. Leite, C.M.O. Raposo, S.M.L. Silva, Caracterização estrutural de argilas bentoníticas nacional e importada: antes e após o processo de organofilização para utilização como nanocargas, Cerâmica 54 (2008) 303–308.